Proceedings of ASME Turbo Expo 2011
GT2011
June 6-10, 2011, Vancouver, British Columbia, Canada

GT2011-45221

FURTHER CHARACTERIZATION OF THE DISTURBANCE FIELD IN A TRANSVERSELY EXCITED SWIRL-STABILIZED FLAME

Jacqueline O'Connor, Tim Lieuwen
Georgia Institute of Technology
Atlanta, Georgia, USA

ABSTRACT

Transverse instabilities in annular gas turbine combustors are an important problem for both power generation and aircraft applications. These instabilities, also found in afterburners and rocket engines, are manifested as strong acoustic field fluctuations perpendicular to the flow direction. Transverse acoustic waves not only directly perturb the flame, but also couple with nozzle acoustics and inherent fluid mechanic instabilities. As such, the unsteady flow field that disturbs the flame is a complex superposition of transverse and longitudinal disturbances associated with both acoustic and vortical waves. This study closely follows prior work of the authors, which overviewed the disturbance field characteristics of a transversely forced, swirling nozzle flow. Velocity data from a transversely forced, swirl-stabilized flame was taken using high-speed particle image velocimetry (PIV). The topology of the velocity and vorticity field is compared between the in-phase and out-of-phase forcing cases using both filtered and instantaneous data. These data also show that the acoustic and vortical disturbances are comparable in amplitude and, because they propagate at very different speeds, their superposition leads to prominent interference patterns in the fluctuating velocity. Data from both non-reacting and reacting test cases are presented to show that many features of the unsteady shear layers are quite similar.

NOMENCLATURE

A_1	Amplitude of acoustic wave (model)
A_2	Amplitude of vortical wave (model)
D	Outer diameter of the swirler nozzle
S	Nozzle annular area
f_o	Forcing frequency
$\dot{m}$	Mass flow
r	Radius
t	Time
u_o	Bulk velocity
$u_{c,v}$	Convection velocity
u'	Axial velocity fluctuation
$\hat{u}$	Fourier transform of axial velocity fluctuations
v'	Transverse velocity fluctuation
$\hat{v}$	Fourier transform of transverse velocity fluctuations
α	Vortical decay rate (model)
ρ	Density
ϕ	Phase of vorticity
φ	Phase difference (model)
ω	Angular frequency

INTRODUCTION

Combustion dynamics, a coupling between resonant combustor acoustics and flame heat release fluctuations, has been a problem with propulsion and power generation technologies since the middle of the twentieth century [1]. Initially explained by Rayleigh [2], this coupling can lead to high-cycle fatigue and engine damage, reduced operability windows, and increased emissions. For gas turbines, these instabilities have become more pronounced as engines have been optimized for low NO_x emissions [3]. The main emissions abatement strategy, lean combustion, has lead to a rise in the severity of instabilities and the more frequent appearance of transverse instabilities in these engines.

Transverse instabilities are a common instability mode in rockets [4-6], augmenters [7-9], and annular combustors [10, 11], but have only recently become a significant issue for can-annular gas turbine systems [12]. These instabilities are characterized by acoustic pressure and velocity perturbations that oscillate normal to the direction of flow. Traditionally, longitudinal instabilities have been the dominant mode in can-annular engines and significant work has been done to understand the coupling mechanisms [13-15]. More recently, work has been initiated to shed light on some of the flame response characteristics and coupling mechanisms for transversely forced flames [16-22].

Understanding the underlying mechanism for instability is important for explaining the conditions under which instabilities do and do not appear. Two dominant coupling mechanisms in gas turbines are equivalence ratio [23-25] and velocity [26-29] coupling, where other mechanisms, such as pressure coupling [1], are believed to play a negligible role. In this work, we focus on velocity coupled disturbances, by which we mean the flame response to acoustic and vortical velocity perturbations.

Several studies have provided detailed characterizations of the way in which velocity disturbances lead to heat release oscillations. First, acoustic velocity perturbations at the flame attachment point excite flame wrinkles that propagate the entire length of the flame at a speed approximately equal to that of the mean flow [30]. Vortical velocity disturbances, originating from the edge of the nozzle, e.g., the rollup of the separating shear layer or the backward facing step, distort the flame as they propagate axially at the vortex convection speed [31]. Acoustic disturbances also excite wrinkles as they propagate axially and/or transversely at the sound speed. Finally, several researchers have pointed to a swirl fluctuation mechanism that causes the flame angle to fluctuate with the swirl number [32-35]. Put together, the flame is being simultaneously wrinkled by several sources, each with their own phase and convection speeds.

As discussed in O'Connor *et al.* [16], the velocity disturbance field in a transversely forced flame is significantly more complex than in the longitudinal problem. The incident transverse acoustic perturbation disturbs the flame in an intrinsically non-axisymmetric manner. In addition, the acoustic pressure fluctuation over the nozzle leads to longitudinal acoustic fluctuations in the nozzle region, as shown by Staffelbach and coworkers' [18] simulations, and in experiments reported by O'Connor *et al.* [16]. Additionally, vortex roll-up at the base of the flame leads to additional velocity disturbance sources. These disturbance mechanisms and their pathways are represented in Figure 1.

Each of these processes can be described with a transfer function, as is shown in Figure 1. For example, the coupling between acoustic fluctuations at the nozzle and the resulting vortex rollup is characterized using an acoustic to hydrodynamic velocity transfer function. Additionally, the transverse to longitudinal acoustic coupling mechanism provides an interesting connection back to the previous flame transfer function work performed for longitudinally excited flames.

In general, the flame response is due to a superposition of the different effects shown in Figure 1. This superposition manifests in the flame response both locally and globally [27, 32, 34-41]. The experimentally observed rise, dip, and subsequent rise of the flame transfer function with frequency is attributed to constructive and destructive interference between disturbances at different parts of the flame. Similarly, the spatial distribution of the flame response can be explained in the same way. Shanbhogue *et al.* [42] show that the response amplitude of the flame, as measured by the flame displacement from the centerline axis, first rises and then falls as a function of downstream distance. Recent studies from Emerson *et al.* [43] show nodes in the response of a vitiated bluff-body stabilized flame at certain axial locations.

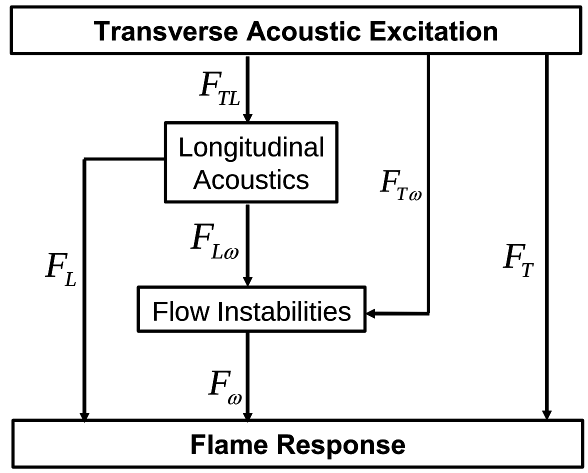

Figure 1. Velocity disturbance mechanisms present in a transversely forced flame.

Interference phenomenon can not only be seen in the flame response, but also in the velocity disturbance field. Acoustic and vortical disturbances travel downstream and constructively and destructively interfere. This interference effect is particularly striking when the two disturbances are of similar amplitudes. If the amplitudes of the two waves are roughly equal, the nodes in the interference pattern are approximately zero, resulting in a zero velocity fluctuation in certain spatial locations. This effect was briefly discussed in O'Connor *et al.* [16] and is more thoroughly investigated in this work.

We next consider the unsteady flow field characteristics in swirling flow in more detail. Swirl flows exhibit a bewildering variety of behaviors depending upon geometry, swirl number, Reynolds number, and many other parameters. Indeed, it is currently not possible to draw general conclusions about flow structure from specific papers, as results are highly configuration specific. Moreover, it appears that a general flow classification for the type of unsteady flow structures, their mechanism of occurrence, and how they manifest themselves, does not exist yet for swirling flows. Finally, it is known that heat release has important effects upon both the time averaged and unsteady flow structure, so that non-reacting swirl flow results are generally taken to have little or no applicability to reacting flows. For example, the addition of heat release from the flame changes the global stability of the swirling flow, as described by Rusak *et al.* [44]. This results in a change in the critical swirl number as well as the shape and dynamics of the vortex breakdown region. However, as alluded to in an earlier study by the authors [16], we found many qualitative similarities in unsteady shear layer structures between the reacting and non-reacting flows. The rest of this introduction outlines our working hypothesis used to interpret data presented here.

The time averaged flow field essentially forms the "base" flow state shown in Figure 2a, upon which disturbances are initiated, grow, or decay. This "base" state for high swirl number flows basically consists of an outer flow passing around a vortex breakdown bubble. Heat release has significant influences upon this "base" state – for example, the width and length of the vortex breakdown bubble. In addition, it influences the axial location of its stagnation points and the spreading angle of the annular jet exiting the nozzle.

Now consider the unsteady flow structures. In a swirling flow with vortex breakdown, several different sources of instability coexist. Vortex breakdown is a manifestation of an absolute instability of the swirling jet. In other words, the vortex breakdown region, characterized above as a flow feature controlling the "base" state in the central part of the flow field, is itself intrinsically unsteady. The shear layers, in both the azimuthal and streamwise directions, are convectively unstable, which results in their rollup. This shear layer rollup is shown in Figure 2b.

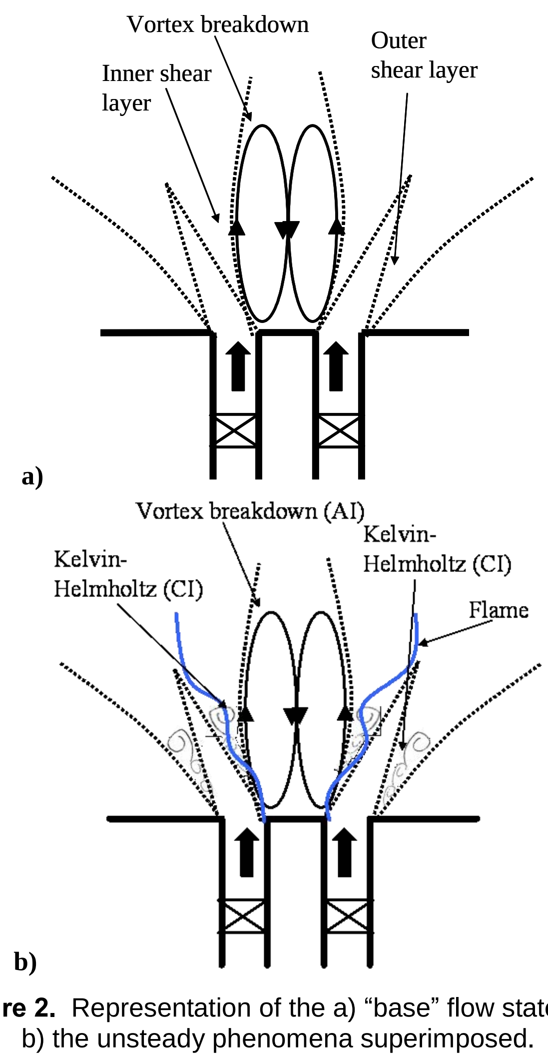

Figure 2. Representation of the a) "base" flow state and b) the unsteady phenomena superimposed.

We postulate that the distinction between the absolutely unstable (AI) vortex breakdown bubble and convectively unstable (CI) shear layers is key to understanding the response of the system to low to intermediate amplitude acoustic excitation. The absolutely unstable breakdown bubble exhibits intrinsic dynamics that are relatively independent of low amplitudes of excitation [45, 46]. Therefore, the basic dynamics of this flow remains unchanged in the presence of low amplitude acoustic forcing. Only in the presence of large amplitude dynamics that alter the vortex breakdown bubble [47] and cause frequency locking of bubble dynamics are the interactions between the excitation and vortex breakdown bubble dynamically significant, although this effect too may be limited to a change in the time averaged "base" state.

The convectively unstable shear layers are amplifiers that respond to the external forcing. Moreover, since the flame lies in the shear layer, as shown in Figure 2b, the instability characteristics of the shear layers dominate the flame response. Also, although the "base" state of the flow changes with heat release, the essential features of the unstable shear layers do not. This implies that key dynamical features of the flow that excite the flame remain qualitatively similar between non-reacting and reacting situations. This point should not be pressed to far, as heat release certainly has important influences on the shear layer development. For example, the dilatation effect of heat release acts as a vorticity sink in the inner shear layer where the flame is stabilized.

Nonetheless, a key hypothesis put forward here is that the key unsteady flow features responsible for disturbing the flame are essentially the same between reacting and non-reacting flow configurations. In the rest of this paper, we further investigate the velocity disturbance field characteristics in a transversely forced annular swirling jet, both for non-reacting and reacting flows. First, we discuss the experimental configuration and diagnostic systems used. Next, an overview of the important disturbance field characteristics is outlined. This is followed by a more detailed look at the convection velocity, mode shape, and relative amplitude of the disturbances in the flow field. These parameters are used to develop a two wave model that describes the interference phenomenon observed in the fluctuating velocity field.

EXPERIMENTAL SETUP

In this section we overview the experimental facility and diagnostic systems used in this study. For more experimental facility details, see O'Connor *et al.* [16].

The combustor mimics an annular combustor configuration and was designed to support a strong transverse acoustic mode. A swirler nozzle is situated at the center of the chamber with an outer diameter of 31.75 mm, inner diameter of 21.84 mm, and swirl number of 0.85. The fuel is natural gas and the equivalence ratio is 0.9. Six acoustic drivers, three on each side, provide the acoustic excitation for the system. The system is show in Figure 3.

Figure 3. Transverse forcing facility.

The acoustic drivers on either side of the combustor can be controlled independently. By changing the phase between the signals driving each side of the combustor, different wave patterns, both standing and traveling waves, can be created. When the drivers are forced in-phase, a pressure anti-node and velocity node are created at the center of the experiment. When the drivers are forced out-of-phase, a pressure node and velocity anti-node are created at the center. The difference between these acoustic driving conditions can be seen in the data by looking at the transverse velocity along the centerline. In the case of out-of-phase forcing, the centerline velocity is high amplitude and sinusoidal, where in the in-phase forcing case, the signal is random and low amplitude. The non-zero value of the transverse velocity observed for the in-phase case is likely due to slight imbalances in excitation amplitudes of the left and right speakers and random motion in the vortex breakdown region.

Particle image velocimetry is used to measure the velocity field in this experiment. A LaVision Flowmaster Planar Time Resolved system allows for two-dimensional velocity measurements at 10 kHz.

All results are presented in non-dimensional form. The velocities are normalized by the bulk approach flow velocity, $\dot{m}/\rho S$ (where ρ and S denote approach flow density and annulus area), the spatial coordinates by the nozzle diameter, D, time by the forcing frequency, f_o, and the vorticity by the bulk velocity divided by the annular gap width, $U_o/(r_2-r_1)$.

RESULTS

This section contains three parts: explanation of the time-average flow properties, an overview of the disturbance flow field topology, and a discussion of the fluctuating disturbance field characteristics and the interference behavior found within.

The time-averaged axial velocity and out-of-plane vorticity are shown in Figure 4, with the non-reacting flow on top and reacting on bottom. The time-averaged flow fields of the non-reacting and reacting cases are different in several ways. First, the vortex breakdown bubble changes in size and shape, growing wider at the dump plane in the reacting case. Second, the jet spreading angle is higher in the reacting case, presumably because of the expansion of the vortex breakdown bubble. Third, the average shear layer locations, as shown by the vorticity plots, also spread as a result of the two aforementioned effects. Note that this flow contains two distinct shear layers, one emanating from the inner edge and one from the outer edge of the annulus. The flame configuration is nominally in a V-shape flame, stabilized in the inner shear layer.

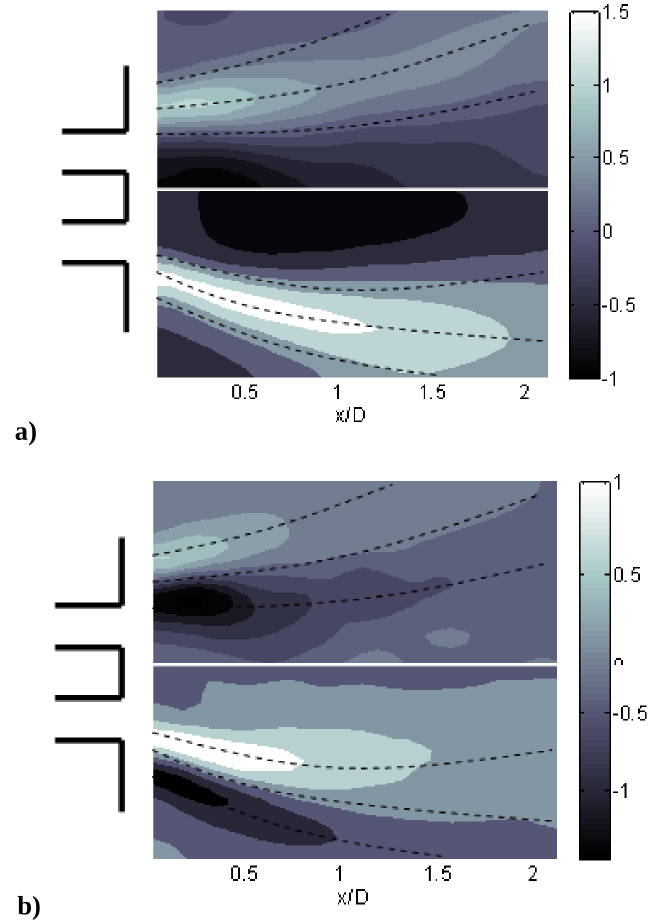

Figure 4. Time-averaged a) axial velocity and b) vorticity in non-reacting (top) and reacting (bottom) flow. Bulk velocity is U_o=10 m/s. Dotted lines represent nominal jet centers and shear layer paths.

Flow field topology

At a given mean flow velocity, the vorticity field is a function of the acoustic forcing configuration and the presence of a flame. First, the effect of acoustic forcing is considered. The transverse acoustic velocity causes significant side-to-side flow field and flame motion. Additionally, the transverse acoustics create pressure disturbances that, as described above, lead to axial velocity fluctuations at the nozzle. The phasing of these axial fluctuations on either side of the nozzle determines the symmetry of the disturbance field. Figure 5 shows a notional sketch of a cross-section of the flow field.

The figure shows three main feature of the flow field in both the reacting and non-reacting flow. First, the center of the flow is dominated by the vortex breakdown bubble. On either side of the bubble is the annular jet column. The inner shear layer, the region of shear between the jet column and the vortex breakdown region, and the outer shear layer, the region between the jet column and the ambient fluid, contain coherent vortices. These structures are formed as a result of fluctuating axial velocity at the nozzle, and the phase of the fluctuations on one edge with respect to the other edges determines the symmetry of the vorticity field.

Figure 5a shows the case of an asymmetric flow field, caused by out-of-phase acoustic forcing. Here, a helical pattern is created within each shear layer, resulting in a staggered vortex pattern in the plane formed by the laser sheet. Figure 5b shows an example of an axisymmetric flow field, where vortex rings propagate downstream from the inner and outer edges of the annulus. As they convect downstream, these structures deform and locally bend the jet column. In addition to the aforementioned processes, the transverse acoustic motion periodically shifts the flow field from side to side, shifting the angle of the jet column and the trajectories of the coherent structures.

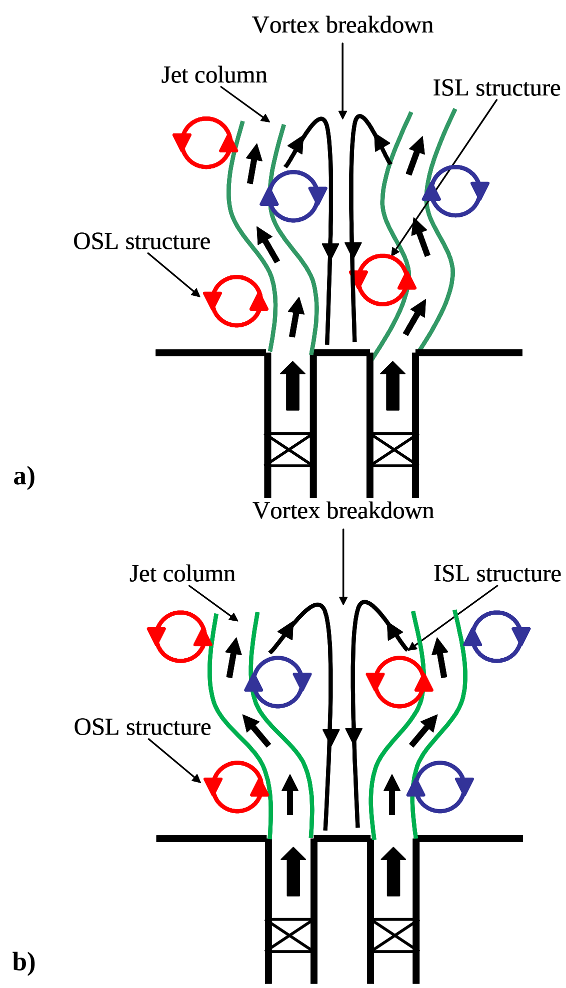

Figure 5. Notional picture of the flow field for a transversely forced swirling jet with a) out-of-phase and b) in-phase acoustic forcing. Coherent structures in the inner shear layer (ISL) and outer shear layer (OSL) travel downstream, bending the jet column as they pass.

The plots in Figure 6 show the filtered velocity and vorticity field by plotting the sum of the fluctuation of the vorticity at the forcing frequency and the mean vorticity. This calculation, similar to the analysis described in Ref. [16], involves taking the FFT of the instantaneous velocity and vorticity at each point and harmonically reconstructing the signal at the forcing frequency. This is effectively a filtering, or phase locking, process that captures only the motions at the forcing frequency, eliminating turbulent noise. This process also spatially smears out the instantaneous vorticity, due to cycle-cycle phase jitter in axial location of the vortical structures. Figure 6, like the notional pictures in Figure 5, shows the out-of-phase and in-phase velocity and vorticity fields for one phase of the acoustic cycle.

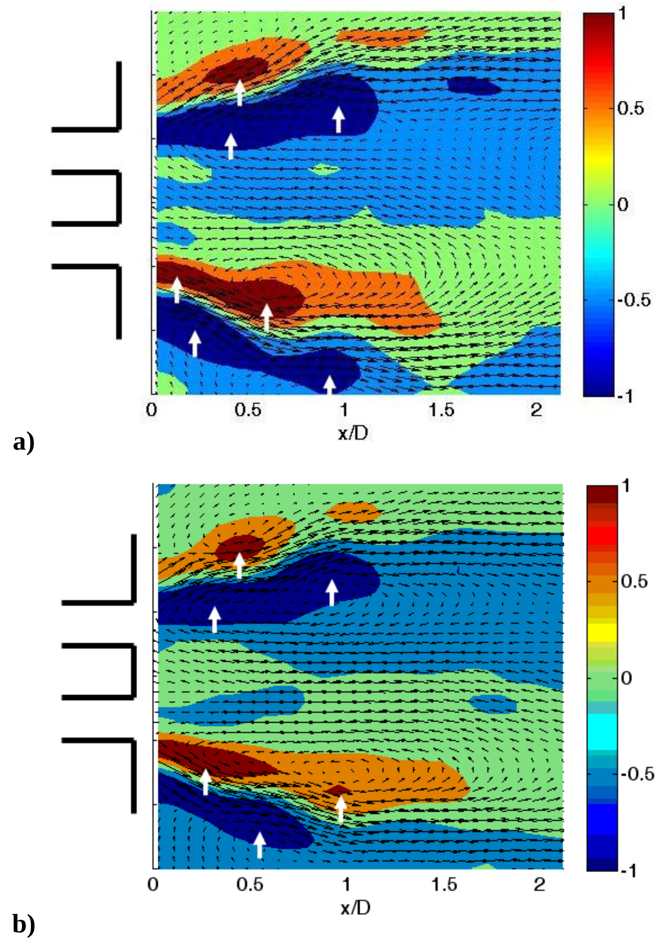

Figure 6. Normalized filtered velocity and vorticity field for a) out-of-phase and b) in-phase acoustic forcing for reacting flow at a bulk velocity of U_o=10 m/s and a forcing frequency of f_o=400Hz.

In the out-of-phase forcing case, a pressure node is present along the centerline of the flow. The pressure fluctuations on either side of the node are out of phase, creating out-of-phase axial velocity fluctuations on either side of the nozzle. This asymmetry in the axial velocity fluctuations leads to an asymmetry in the vorticity field, which is evident in Figure 6a. For example, in the outer shear layer, the structure closest to the dump plane is on the right-hand side at x/D=0.2. The next shear layer structure is on the left-hand side at x/D=0.5. The final structure of significant strength in the outer shear layer is again on the right-hand side at x/D=0.9. This vortex structure suggests a helical vortex pattern in both the inner and outer shear layers, similar to LES simulations by García-Villalba and Frölich [48], shown in Figure 7.

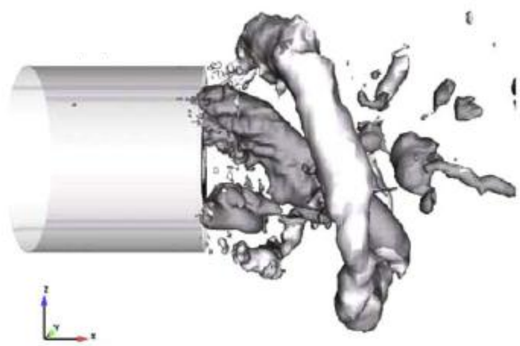

Figure 7. Snapshot of a helical shear layer instability in a swirling annular jet, used to visualize coherent structures from LES simulation [48] under longitudinal, self excited oscillations.

In the in-phase forcing, the formation of structures in each shear layer is nominally axisymmetric. For example, the inner shear layer shows two sets of structures, one located at x/D=0.3 and one at x/D=0.9. The outer shear layer structures are also axisymmetric, but not aligned with the structures in the inner shear layer. Similar trends for both the in-phase and out-of-phase forcing are observed in the non-reacting cases as well.

The behavior of the vorticity field in these filtered velocity and vorticity images is very similar to that of the instantaneous fields, show in Figure 8. The harmonic reconstruction acts as a phase-locking process that smears the effect of phase jitter and neglects the motions at other frequencies. Despite that, the major coherent features of the flow are similar. The images chosen for Figure 8 correspond to the phases depicted in Figure 6.

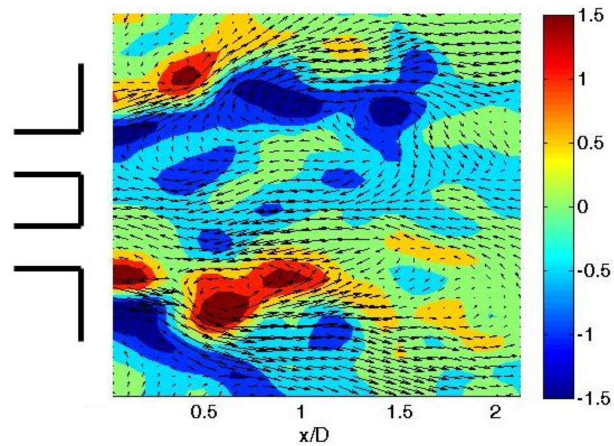

a)

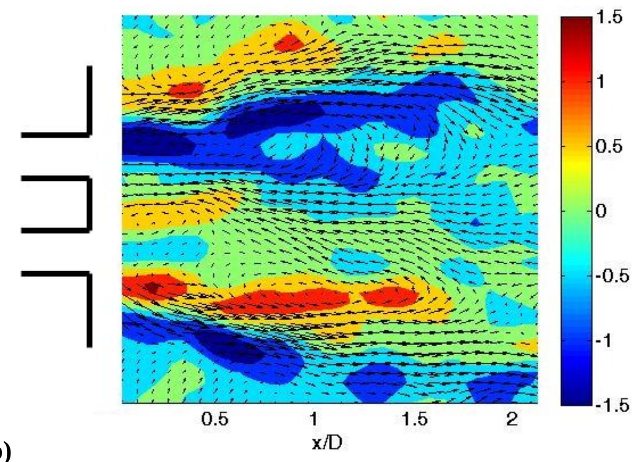

b)

Figure 8. Instantaneous normalized velocity and vorticity fields for a) out-of-phase and b) in-phase acoustic forcing for reacting flow at a bulk velocity of U_o=10 m/s and a forcing frequency of f_o=400Hz.

The local behavior and downstream evolution of the shear layer structures appear qualitatively similar between the non-reacting and reacting cases, further emphasizing the point that heat release does not affect the basic mechanisms responsible for the appearance of unsteady flow structures in the shear layers that distort the flame. The major difference between the two is difference in dissipation rate of the vorticity. In the reacting case, significant coherent structures are seen until x/D=1, where the coherent structures have decayed by x/D=0.4 in the non-reacting case.

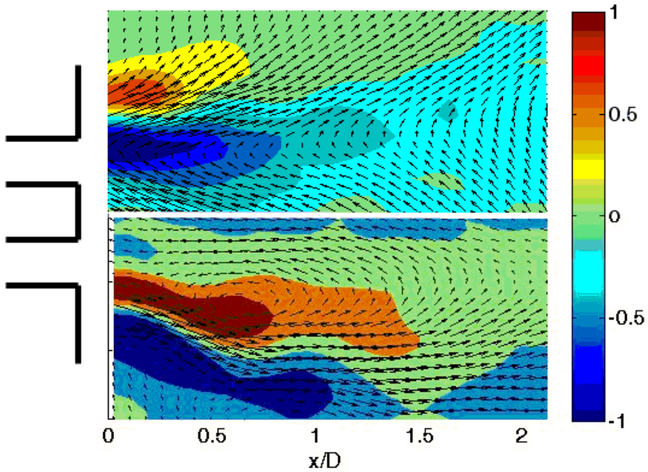

Figure 9. Comparison of the normalized filtered velocity and vorticity field between non-reacting (top) and reacting (bottom) flows at a bulk velocity of U_o=10 m/s and a forcing frequency of f_o=400 Hz out-of-phase.

Convection velocities of the vortex structures were estimated from the axial phase dependence of the vortical disturbances shown in Figure 10. These phases were calculated from the phase of the FFT at the forcing frequency along the inner and outer shear layers, as shown in Figure 4. The shear layer locations were estimated from the time-average vorticity magnitude maxima.

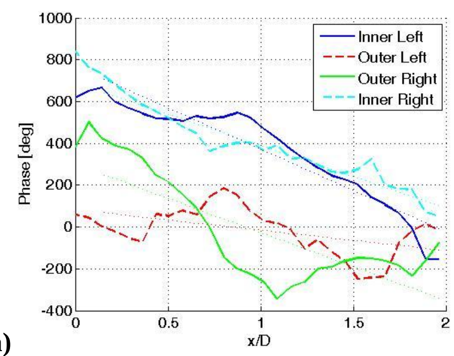

a)

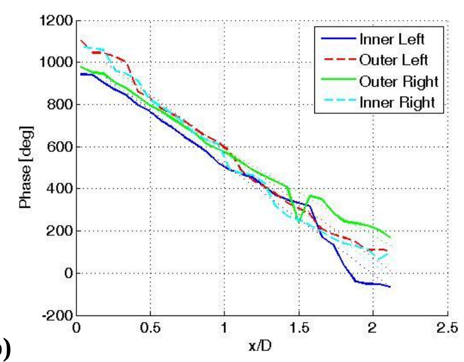

b)

Figure 10. Phase of vorticity along shear layers for a) non-reacting and b) reacting flow at a bulk velocity of U_o=10 m/s and a forcing frequency of f_o=400 Hz out-of-phase.

Linear fits of the phase data were calculated as a function of downstream distance. The slope of this line was taken from the fit and used to calculate the convection velocity using the formula:

$$u_{c,v} = 2\pi f_o \; {}^{1}\!\Big/_{\frac{d\phi}{dx}} \quad (1)$$

The convection speeds of the vorticity along the six lines of travel were calculated and averaged, leading to a value of 13 and 10 m/s for the non-reacting and reacting cases, respectively. Each convection speed falls within the range of convection speeds measured in non-swirling flows, which are ~$0.5U_o$<$u_{c,v}$<~$1.5U_o$ [49]. Additionally, the phase between the disturbances traveling in the jets is shown in Table 1. The uncertainty in phase is ±15 degrees.

Table 1. Average phase difference between vorticity disturbances in the left and right jet centers at several conditions at a bulk velocity of U_o=10 m/s and a forcing frequency of f_o=400 Hz.

	Phase (±15º)
Non-reacting, Out-of-phase	20
Reacting, Out-of-phase	-50
Non-reacting, In-phase	100
Reacting, In-phase	130

These phase differences indicate the shape and symmetry of the disturbance field on either side of the nozzle. For example, the phases of the in- and out-of-phase reacting cases are 130 and -50 degrees, respectively. This can be seen by looking at snapshots of the vorticity field at any point in time, shown in Figure 6.

The meaning of the -50 and 130 degree phase differences are evident from the plots in Figure 6. In Figure 6a, the out-of-phase forcing case, the vortical disturbances are non-axisymmetric. The plot in Figure 6b depicts the in-phase forcing case, which is roughly axisymmetric. Although the vortex pairs are slightly staggered, possibly because of the motion of the swirl, the 130 degree phase between the vorticity fluctuations on either side of the jet indicates that symmetric vortex rings are being formed.

Fluctuating disturbance field characteristics

This section focuses on the unsteady disturbance field characteristics, as opposed to the total instantaneous/filtered field structure detailed earlier. There are fundamental differences between the appearance of the unsteady flow structures as visualized by their instantaneous and fluctuating values. For example, the location and characteristics of vortical structures can look fundamentally different between the two, and conclusions about topological flow features should probably only be drawn from the total, instantaneous or filtered field characteristics. That said, the unsteady flame response is closely linked to these fluctuating quantities. In this section, we look only at the fluctuating quantities, by subtracting the time-average behavior, to more carefully investigate the behavior of the different velocity disturbances in the flow field.

Surface plots of the amplitude of both the velocity and vorticity fluctuations show interesting results. Figure 11, Figure 12, and Figure 13 show the amplitude of the axial velocity, transverse velocity, and vorticity fluctuations at the forcing frequency, respectively, for both non-reacting and reacting flow.

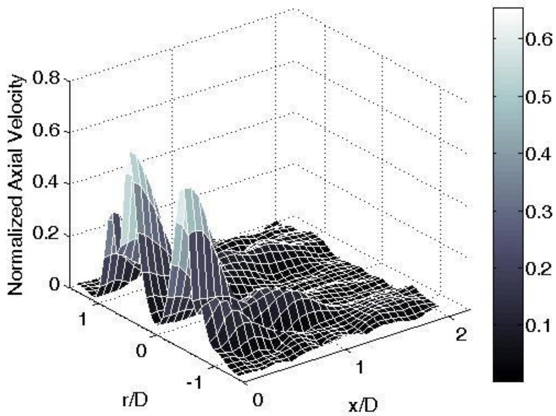

a)

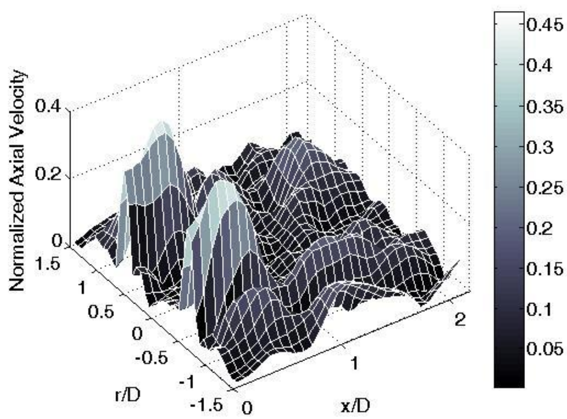

b)

Figure 11. Normalized amplitude of axial velocity fluctuations for a) non-reacting and b) reacting flow at the forcing frequency at a bulk velocity of U_o=10 m/s and a forcing frequency of f_o=400 Hz out-of-phase.

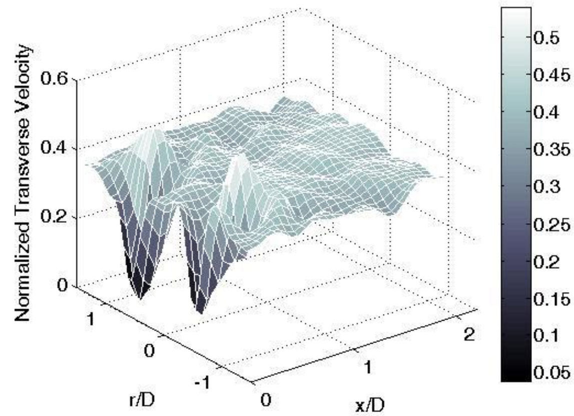

a)

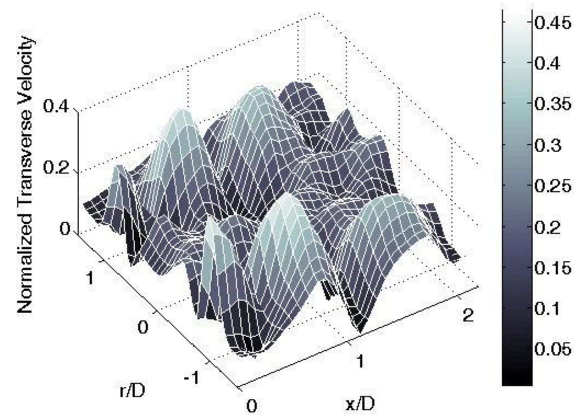

b)

Figure 12. Normalized amplitude of transverse velocity fluctuations for a) non-reacting and b) reacting flow at the forcing frequency at a bulk velocity of U_o=10 m/s and a forcing frequency of f_o=400 Hz out-of-phase.

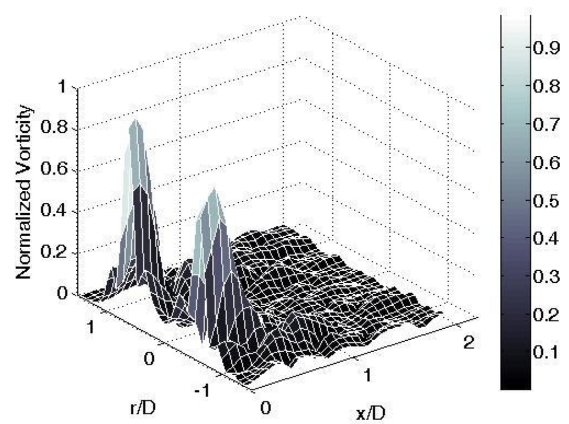

a)

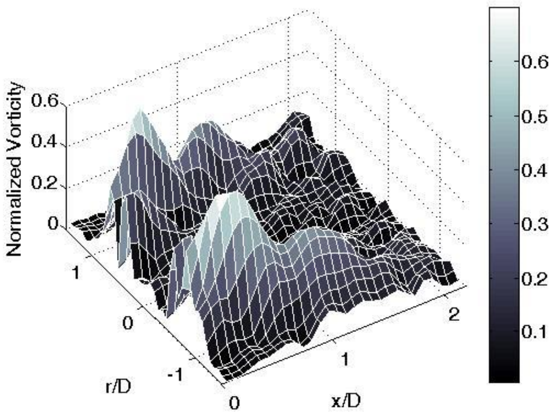

b)

Figure 13. Normalized amplitude of vorticity fluctuations for a) non-reacting and b) reacting flow at the forcing frequency at a bulk velocity of U_o=10 m/s and a forcing frequency of f_o=400 Hz out-of-phase.

One of the most prominent features of these plots is the highly non-monotonic characteristics of the unsteady velocity field, suggesting cancellation phenomenon. For example, in Figure 12b, which shows the transverse velocity fluctuations at the forcing frequency for a reacting case, the fluctuation amplitude peaks at approximately *x/D*=0, decreases to a minimum value at *x/D*=0.3, and then increases until a downstream distance of *x/D*=0.6 where it again peaks and decreases.

While both the axial and transverse velocity fluctuation fields show the interference phenomenon, there is another important factor that differentiates these two types of fluctuations. The transverse velocity fluctuation surface, shown in Figure 12, has a constant offset across the field. This offset is a result of the acoustic velocity fluctuations, which are of nearly constant amplitude across the field of view for the out-of-phase forcing case shown. Conversely, there is no offset of the axial velocity surfaces, indicating that there are no longitudinal acoustics in the flow field downstream of the immediate nozzle exit. Thus, longitudinal acoustics are important in the immediate vicinity of the nozzle, but these fluctuations do not contribute in any significant way farther into the combustor.

We believe that the non-monotonic spatial dependence of velocity amplitude is due to the simultaneous presence of both acoustic and vortical velocity disturbances. This can be shown by constructing a simple model of the unsteady transverse velocity field, with disturbances propagating at two different axial phase speeds. The input parameters for this model are the initial amplitude of each wave (A_1 and A_2), the decay rate (α) and convection speed (u_c) of the vortical disturbance, and the phase (φ) between the two disturbance types, see Equation 2.

$$u_{acoustic} = A_1 e^{-i\omega t+\varphi}$$
$$u_{vortical} = A_2 e^{-i\omega (t - x/u_{c,v})} e^{-\alpha x} \qquad (2)$$

The convection velocity of the vortical wave was estimated from the mean of the velocities calculated from Equation 1. The decay rate was then calculated by fitting an exponential to the decay of time-average vorticity as a function of downstream distance, the results of which can be seen in Figure 14. This was done for both the non-reacting and the reacting case.

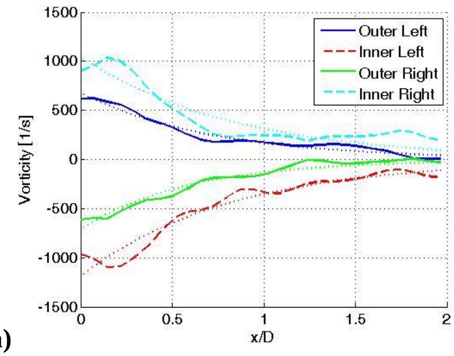

a)

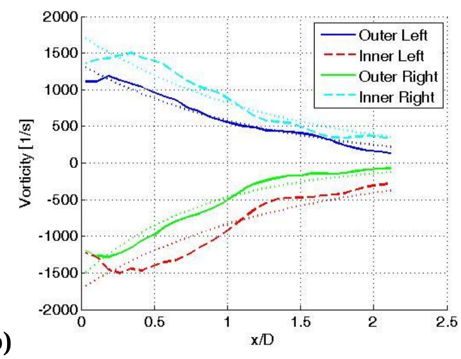

b)

Figure 14. Time-average vorticity in shear layers for the a) non-reacting and b) reacting cases at a bulk velocity of U_o=10 m/s and a forcing frequency of f_o=400 Hz out-of-phase. Dotted lines indicate exponential curve fits to calculate decay rates with downstream distance.

The parameters for the acoustic wave were less obvious to extract from experimental data and were used as fit parameters to match the data. The parameters used in the model for both the non-reacting and reacting cases are shown in Table 2.

Table 2. Two-wave model conditions for non-reacting and reacting cases at 400 Hz out-of-phase acoustic forcing and 10 m/s bulk flow velocity.

	Non-reacting	**Reacting**
A_1	0.3	0.25
φ	$\pi/6$	$\pi/4$
A_2	0.3	0.25
α [1/m]	43	27
$u_{c,v}$ [m/s]	13	10

The results of both the data and the model in the non-reacting and reacting cases are as shown in Figure 15.

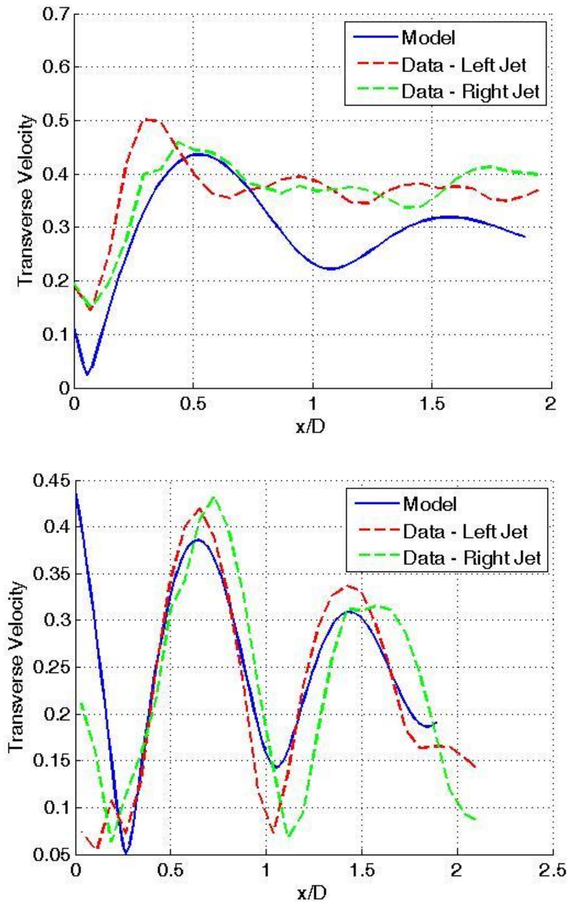

a)

b)

Figure 15. Comparison of transverse velocity fluctuation amplitude in left and right jet of the a) non-reacting and b) reacting data and the two-wave interaction model. The bulk velocity was U_o=10 m/s and the forcing frequency was f_o=400 Hz out-of-phase

As can be seen from Figure 15, the results of the data and the model align reasonably well. An important feature of these graphs is the peak spacing in the interference pattern, which is only a function of the difference in acoustic and vortical phase velocities. This is captured quite well in the model.

An important implication of this model is that the amplitudes of the acoustic and vortical wave are essentially the same. For example, both the acoustic and vortical fluctuations in the reacting case, shown in Figure 15b, are 25% of the bulk flow velocity. This result has important implications on flame response modeling, as models often assume that it is the vortical disturbances that dominate the flame response [42]. These results show that the acoustic and vortical disturbances have comparable magnitudes. This result reinforces the complexity of disturbance field and while the mechanisms do have causal relationships, as shown in Figure 1, they co-exist and combine to create a complex disturbance field.

These results also speak to the amplitude and phase of $F_{T\omega}$, the transfer function that describes the relationship between the transverse acoustic motion and the vortex rollup at the nozzle, as shown in Figure 1. The ratio of the amplitudes, A_1 and A_2, gives the magnitude of the transfer function at this particular forcing frequency, while the phase between the two disturbances, Φ, is the phase of the transfer function at the forcing frequency. Note that this results suggests then, that $F_{T\omega} \sim 1$.

CONCLUSIONS

The aim of this study was to continue the investigation of the velocity disturbance field of a transversely excited swirl-stabilized flame. Discussion of the flow field topology was expanded by considering the changes in the unsteady characteristics of the flow between in-phase and out-of-phase acoustic forcing, as well as non-reacting and reacting flows. In both the non-reacting and reacting flow, the disturbance field shows an interference pattern at the forcing frequency, which is caused by the constructive and destructive interference of acoustic and vortical disturbances. A model was developed to explain this phenomenon and compare with the data.

There are several conclusions that can be drawn from this work.

1. The disturbance field consists of a series of velocity disturbances with causal relationships described in the disturbance pathway diagram in Figure 1. The transverse acoustic pressure fluctuations result in mass flow fluctuations at the nozzle. This axial motion causes fluctuations in the vortex sheet strength.
2. The resulting disturbance field is dominated by two types of disturbances, acoustic and vortical. These disturbances constructively and destructively interfere to cause interference patterns in the velocity field.
3. Out-of-phase forcing cases result in asymmetric vorticity disturbances, presumably associated with a helical structure, while in-phase forcing results in nominally axisymmetric vortical structure.
4. Using convection velocity and decay rate parameters calculated from the vorticity data, a model assuming superposition of acoustic and vortical disturbances captures the interference pattern in the velocity data. The important parameter, the peak spacing in the interference pattern, is well captured in both the non-reacting and reacting cases.

ACKNOWLEDGMENTS

This work has been partially supported by the US Department of Energy under contracts DEFG26-07NT43069 and DE-NT0005054, contract monitors Mark Freeman and Richard Wenglarz, respectively.

REFERENCES

1. Ducruix, S., Schuller, T., Durox, D., and Candel, S., *Combustion dynamics and instabilities: Elementary coupling and driving mechanisms.* Journal of Propulsion and Power, 2003. **19**(5): p. 722-734.
2. Rayleigh, L., *The Theory of Sound*. 2 ed. Vol. 2. 1896, London: Macmillian.
3. Lieuwen, T. and V. Yang, *Combustion Instabilities in Gas Turbine Engines: Operational Experience, Fundamental Mechanisms, and Modeling*. Progress in Astronautics and Aeronautics Series, ed. F.K. Lu. 2006: AIAA.
4. Culick, F.E.C. and V. Yang, *Prediction of the stability of unsteady motions in solid propellant rocket motors.* Nonsteady Burning and Combustion Stability of Solid Propellants, 1992: p. 719.
5. Harrje, D.T. and F.H. Reardon, *Liquid propellant rocket combustion instability*. 1972: Scientific and Technical Information Office, National Aeronautics and Space Administration.
6. Price, E.W., *Solid Rocket Combustion Instability—An American Historical Account.* Nonsteady Burning and Combustion Stability of Solid Propellants, 1992: p. 1-16.
7. Rogers, D.E. and F.E. Marble, *A mechanism for high frequency oscillations in ramjet combustors and afterburners.* Jet Propulsion, 1956. **26**(1): p. 456–462.
8. Kaskan, W.E. and A.E. Noreen, *High-frequency oscillations of a flame held by a bluff body.* ASME Transactions, 1955. **77**(6): p. 855-891.
9. Elias, I., *Acoustical Resonances Produced by Combustion of a Fuel-Air Mixture in a Rectangular Duct.* The Journal of the Acoustical Society of America, 1959. **31**: p. 296.
10. Smith, K. and J. Blust, *Combustion Instabilities in Industrial Gas Turbines: Solar Turbines' Experience*, in *Combustion Instabilities in Gas Turbine Engines*, T. Lieuwen and V. Yang, Editors. 2005, AIAA: Washington D.C. p. 29-42.
11. Krebs, W., S. Bethke, J. Lepers, P. Flohr, and B. Prade, *Thermoacoustic Design Tools and Passive Control: Siemens Power Generation Approaches*, in *Combustion Instabilities in Gas Turbine Engines*, T. Lieuwen and V. Yang, Editors. 2005, AIAA: Washington D.C. p. 89-112.
12. Sewell, J. and P. Sobieski, *Monitoring of Combustion Instabilities: Calpine's Experience*, in *Combustion Instabilities in Gas Turbine Engines*, T. Lieuwen and V. Yang, Editors. 2005, AIAA: Washington D.C. p. 147-162.
13. Hield, P.A., M.J. Brear, and S.H. Jin, *Thermoacoustic limit cycles in a premixed laboratory combustor with open and choked exits.* Combustion and Flame, 2009. **156**(9): p. 1683-1697.
14. Paschereit, C.O., E. Gutmark, and W. Weisenstein, *Excitation of thermoacoustic instabilities by interaction of acoustics and unstable swirling flow.* AIAA Journal, 2000. **38**(6): p. 1025-1034.
15. Cohen, J. and W. Proscia, *Characterization and Control of Aeroengine Combustion Instability: Pratt & Whitney and NASA Experience*, in *Combustion Instabilities in Gas Turbine Engines*, T. Lieuwen and V. Yang, Editors. 2005, AIAA: Washington D.C. p. 113-146.
16. O'Connor, J., S. Natarajan, M. Malanoski, and T. Lieuwen, *Disturbance Field Characteristics of a Transversely Excited Annular Jet*, in *ASME Turbo Expo*. 2010: Glasgow, Scotland.
17. Hauser, M., M. Lorenz, and T. Sattelmayer. *Influence of Transversal Acoustic Excitation of the Burner Approach Flow on the Flame Structure*. in *ASME Turbo Expo*. 2010. Glasgow, Scotland.
18. Staffelbach, G., L.Y.M. Gicquel, G. Boudier, and T. Poinsot, *Large Eddy Simulation of self excited azimuthal modes in annular combustors.* Proceedings of the Combustion Institute, 2009. **32**(2): p. 2909-2916.
19. Wolf, P., G. Staffelbach, A. Roux, L. Gicquel, T. Poinsot, and V. Moureau, *Massively parallel LES of azimuthal thermo-acoustic instabilities in annular gas turbines.* Comptes Rendus Mecanique, 2009. **337**: p. 385-394.
20. Stow, S.R. and A.P. Dowling. *Low-order modelling of thermoacoustic limit cycles*. in *ASME Turbo Expo*. 2004. Vienna, Austria.
21. Acharya, V., Shreekrishna, Shin, D., and Lieuwen, T., *Response of Premixed Swirling Flames to Transverse Excitation*, in *2009 Fall Technical Meeting Organized by the Eastern States Section of the Combustion Institute*. 2009: College Park, MD.
22. Ducruix, S., C. Rey, and S. Candel, *A method for the transverse modulation of reactive flows with application to combustion instability.* Combustion Theory and Modelling, 2005. **9**(1): p. 5-22.
23. Lee, H.J., K.T. Kim, J.G. Lee, B.D. Quay, and D.A. Santavicca. *An Experimental Study on the Coupling of Combustion Instability Mechanisms in a Lean Premixed Gas Turbine Combustor*. in *ASME Turbo Expo*. 2009. Orlando, FL.
24. Birbaud, A.L., S. Ducruix, D. Durox, and S. Candel, *The nonlinear response of inverted "V" flames to equivalence ratio nonuniformitie.* Combustion and Flame, 2008. **154**(3): p. 356-367.
25. Sattelmayer, T., *Influence of the combustor aerodynamics on combustion instabilities from equivalence ratio fluctuations.* Journal of Engineering for Gas Turbines and Power, 2003. **125**: p. 11.
26. Poinsot, T.J., Trouve, A. C., Veynante, D. P., Candel, S. M., and Esposito, E. J., *Vortex-driven acoustically coupled combustion instabilities.* Journal of Fluid Mechanics, 2006. **177**: p. 265-292.

27. Preetham, H. Santosh, and T. Lieuwen, *Dynamics of Laminar Premixed Flames Forced by Harmonic Velocity Disturbances.* Journal of Propulsion and Power, 2008. **24**(6).
28. Schadow, K.C. and E. Gutmark, *Combustion instability related to vortex shedding in dump combustors and their passive control.* Progress in Energy and Combustion Science, 1992. **18**(2): p. 117-132.
29. Ghoniem, A.F., S. Park, A. Wachsman, A. Annaswamy, D. Wee, and H.M. Altay, *Mechanism of combustion dynamics in a backward-facing step stabilized premixed flame.* Proceedings of the Combustion Institute, 2005. **30**(2): p. 1783–1790.
30. Hemchandra, S., N. Peters, and T. Lieuwen, *Heat release response of acoustically forced turbulent premixed flames-role of kinematic restoration.* Proceedings of the Combustion Institute, 2011. **33**(1): p. 1609-1617.
31. McManus, K.R., U. Vandsburger, and C.T. Bowman, *Combustor performance enhancement through direct shear layer excitation.* Combustion and Flame, 1990. **82**(1): p. 75–92.
32. Palies, P., D. Durox, T. Schuller, and S. Candel, *The combined dynamics of swirler and turbulent premixed swirling flames.* Combustion and Flame, 2010. **157**: p. 1698-1717.
33. Komarek, T. and W. Polifke. *Impact of swirl fluctuations on the flame response of a prefectly premixed swirl burner*. in *ASME Turbo Expo*. 2009. Orlando, FL.
34. Gentemann, A., C. Hirsch, K. Kunze, F. Kiesewetter, T. Sattelmayer, and W. Polifke. *Validation of flame transfer function reconstruction for perfectly premixed swirl flames*. in *ASME Turbo Expo*. 2004. Vienna, Austria.
35. Hirsch, C., D. Fanaca, P. Reddy, W. Polifke, and T. Sattelmayer. *Influence of the swirler design on the flame transfer function of premixed flames*. in *ASME Turbo Expo*. 2005. Reno, NV.
36. Kim, D., J.G. Lee, B.D. Quay, D.A. Santavicca, K. Kim, and S. Srinivasan, *Effect of flame structure on the flame transfer function in a premixed gas turbine combustor.* Journal of Engineering for Gas Turbines and Power, 2010. **132**: p. 021502.
37. Shin, D.H., S.J. Shanbhogue, and T. Lieuwen. *Premixed Flame Kinematics in an Axially Decaying, Harmonically Oscillating Vorticity Field*. in *44th AIAA Joint Propulsion Conference*. 2008. Hartford, CT.
38. Preetham and T. Lieuwen. *Nonlinear Flame-Flow Transfer Function Calculations: Flow Disturbance Celerity Effects Part 2*. in *43rd AIAA Aerospace Sciences Meeting and Exhibit*. 2005. Reno, NV.
39. Lieuwen, T., *Modeling Premixed Combustion-Acoustic Wave Interactions: A Review.* Journal of Propulsion and Power, 2003. **19**(5): p. 765-781.
40. Durox, D., T. Schuller, N. Noiray, and S. Candel, *Experimental analysis of nonlinear flame transfer functions for different flame geometries.* Proceedings of the Combustion Institute, 2009. **32**: p. 1391-1398.
41. Freitag, E., H. Konle, M. Lauer, C. Hirsch, and T. Sattelmayer. *Pressure influence on the flame transfer function of a premixed swirling flame*. in *ASME Turbo Expo*. 2006. Barcelona, Spain.
42. Shanbhogue, S., D.H. Shin, S. Hemchandra, D. Plaks, and T. Lieuwen, *Flame sheet dynamics of bluff-body stabilized flames during longitudinal acoustic forcing.* Proceedings of the Combustion Institute, 2009. **32**(2): p. 1787-1794.
43. Emerson, B., U.M. Mondragon, C.T. Brown, V. Acharya, D.-H. Shin, V.G. McDonell, and T. Lieuwen. *Measurements and Analysis of Bluff Body Flame Response to Transverse Excitation*. in *AIAA 49th Aerospace Sciences Meeting and Exhibit*. 2011. Orlando, FL.
44. Rusak, Z., A.K. Kapila, and J.J. Choi, *Effect of combustion on near-critical swirling flow.* Combustion Theory and Modeling, 2002. **6**(4): p. 625-645.
45. Wang, S., S.Y. Hsieh, and V. Yang, *Unsteady flow evolution in swirl injector with radial entry. I. Stationary conditions.* Physics of Fluids, 2005. **17**: p. 045106.
46. Wang, S. and V. Yang, *Unsteady flow evolution in swirl injectors with radial entry. II. External excitations.* Physics of Fluids, 2005. **17**: p. 045107.
47. Khalil, S., K. Hourigan, and M.C. Thompson, *Response of unconfined vortex breakdown to axial pulsing.* Physics of Fluids, 2006. **18**: p. 038102.
48. García-Villalba, M. and J. Fröhlich, *LES of a free annular swirling jet-Dependence of coherent structures on a pilot jet and the level of swirl.* International Journal of Heat and Fluid Flow, 2006. **27**(5): p. 911-923.
49. Bechert, D. and E. Pfizenmaier, *On wavelike perturbations in a free jet travelling faster than the mean flow in the jet.* Journal of Fluid Mechanics, 1975. **72**(2): p. 341-352.